

# SpanConv: A New Convolution via Spanning Kernel Space for Lightweight Pansharpening

Zhi-Xuan Chen, Cheng Jin, Tian-Jing Zhang, Xiao Wu and Liang-Jian Deng\*

University of Electronic Science and Technology of China, Chengdu, 611731

{zhixuan.chen, cheng.jin}@std.uestc.edu.cn, zhangtianjinguestc@163.com, wxwsx1997@gmail.com, liangjian.deng@uestc.edu.cn

## Abstract

Standard convolution operations can effectively perform feature extraction and representation but result in high computational cost, largely due to the generation of the original convolution kernel corresponding to the channel dimension of the feature map, which will cause unnecessary redundancy. In this paper, we focus on kernel generation and present an interpretable span strategy, named SpanConv, for the effective construction of kernel space. Specifically, we first learn two navigated kernels with single channel as bases, then extend the two kernels by learnable coefficients, and finally span the two sets of kernels by their linear combination to construct the so-called SpanKernel. The proposed SpanConv is realized by replacing plain convolution kernel by SpanKernel. To verify the effectiveness of SpanConv, we design a simple network with SpanConv. Experiments demonstrate the proposed network significantly reduces parameters comparing with benchmark networks for remote sensing pansharpening, while achieving competitive performance and excellent generalization. Code is available at [https://github.com/zhi-xuan-chen/IJCAI-2022\\_SpanConv](https://github.com/zhi-xuan-chen/IJCAI-2022_SpanConv).

## 1 Introduction

High-spatial-resolution (HR) multispectral (MS) images are the database that reflects changes in geographic information. However, satellite sensors cannot provide HR-MS images due to payload and bandwidth constraints. Pansharpening, a task of fusing HR panchromatic (PAN) images with simultaneously captured low-spatial-resolution (LR) MS images to obtain HR-MS images, facilitates various applications, including mineral exploration, agricultural surveying, geological monitoring, etc. Existing pansharpening approaches can be divided into two categories: hand-crafted feature-based methods and deep learning-based methods.

LR-MS and PAN images are frequently represented by features backed with conventional image processing knowledge in hand-crafted feature-based approaches [Lolli *et al.*, 2017;

Vivone, 2019; Vivone *et al.*, 2018]. However, these features have limited representational power due to their simple structure. On the other hand, by virtue of the powerful nonlinear fitting ability of convolutional neural networks (CNNs), deep learning feature-based approaches [Masi *et al.*, 2016; Yang *et al.*, 2017; He *et al.*, 2019; Deng *et al.*, 2021; Jin *et al.*, 2022; T.-J. Zhang and Vivone, 2022] can automatically extract features from training data and express the complex nonlinearity of data. A comprehensive review can be found in [Vivone *et al.*, 2020].

To improve the performance of CNNs, deeper architectures with millions of parameters are proposed while increasing the computational burden. To balance the computational cost and performance of CNNs, several works, such as group convolution [Krizhevsky *et al.*, 2012], deeply separable convolution [Howard *et al.*, 2017] and blueprint separable convolutions (BSCov) [Haase and Amthor, 2020] attempt to form a more advanced convolution module by modifying the representation of convolution kernels. In addition, complex and deep CNNs will have overfitting problem that cannot be ignored, which leads to poor performance of the model in the face of unknown data, limiting its application in real scenarios.

In this paper, we propose a SpanConv module based on SpanKernel, whose generation process is analogous to the spanning process in linear algebra. In detail, we learn the navigated kernels as the basis vectors, then span the kernel space by corresponding coefficients to create a kernel slice along each input channel dimension. We observed that standard-convolution-generalized kernels distribution could depict as a subspace in the kernel space, which inspired us to cut down the number of navigated kernels, thus reducing the computational parameters with trade-offs of accuracy. The contributions of this work are two-fold:

- We construct a kernel space that approximates the standard convolution kernel space through spanning, and remove the possible redundancy of the standard convolution kernel, which significantly reduces the number of parameters. To the best of our knowledge, the proposed SpanConv method has the fewest network parameters (only about 16,000 parameters) while maintaining competitive pansharpening performance.
- We further analyze the proposed SpanConv from the perspective of subspace in linear algebra, and point out the

\*Contact Author

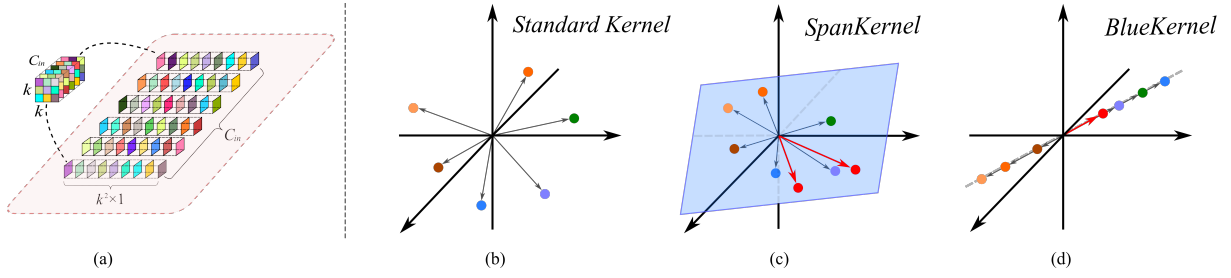


Figure 1: The comparison of standard convolution kernel, the proposed SpanKernel, and prior BlueKernel [Haase and Amthor, 2020]. (a) The standard convolution kernel with  $C_{in} \times k \times k$  is firstly reshaped to  $C_{in}$  kernel vectors with  $k^2 \times 1$ ; Without the loss of generality, we set  $C_{in} = 6$  and  $k^2 = 3$  for the better illustration in  $\mathbb{R}^3$  space. (b) The six kernel vectors are represented by six points in  $\mathbb{R}^3$  space. (c) A  $\mathbb{R}^2$  subspace can be spanned by a linear combination of two independent kernel vectors (*i.e.*, the two red points, also called navigated kernels in this work) in  $\mathbb{R}^3$  space, motivating us to propose the SpanKernel that is further constructing SpanConv. If the six kernel vectors are located in a plane, they can be represented by our SpanKernel completely, thus reducing parameters significantly, especially with larger  $C_{in}$ . (d) A degraded version of our SpanKernel, *i.e.*, the BlueKernel, if the linear combination only has one navigated kernel.

optimal number of navigated kernels by empirical experiments. Also, the better generalization of the given approach is verified comparing with recent state-of-the-art (SOTA) pansharpening techniques.

## 2 Related Works and Motivation

The standard convolution kernel needs to realize the joint mapping of channel correlation and spatial correlation. Its parameters involve spatial and channel dimensions, which are inefficient and prone to redundancy. In AlexNet [Krizhevsky *et al.*, 2012], where group convolution is proposed, the standard convolution procedure is divided into  $g$  sets of smaller sub-operations that can be executed in parallel, thus reducing the computation complexity. In MobileNets [Howard *et al.*, 2017], authors build a simplified architecture through the depth-wise separable convolution (DSC) module. The DSC module decomposes the standard convolution into depthwise convolution and pointwise convolution, thus significantly reducing the parameters. In blueprint separable convolutions (BSConv) [Haase and Amthor, 2020], it is found that many convolution kernels exhibit the same structure after visualizing the learned convolution kernels. Therefore, BSConv uses only a template called a “blueprint” convolution kernel to generate the convolution kernel (denoted as BlueKernel from hereon) and achieves magnificent parameters cut down.

**Motivation.** As the number of convolutional channels increases, learnable parameters dramatically intensify. This problem is unavoidable for deep convolutional neural networks and imposes a tremendous computational load on devices. Naturally, not all parameters are indispensable, which can be observed in the specific pansharpening task. In Fig. 2, we use the standard convolution to replace the SpanConv in our proposed network and reshape the trained kernels into a matrix  $F_i$  (please refer to the definition introduced in Sect. 3.3). Then we apply the principal component analysis (PCA) to the  $F_i$ , and draw the scatter distribution of the first four principal components of each kernel, demonstrating the low rank of  $F_i$ . The results show that the first two components manifest strong representation ability, of which the remaining components are weak. This observation further verifies the

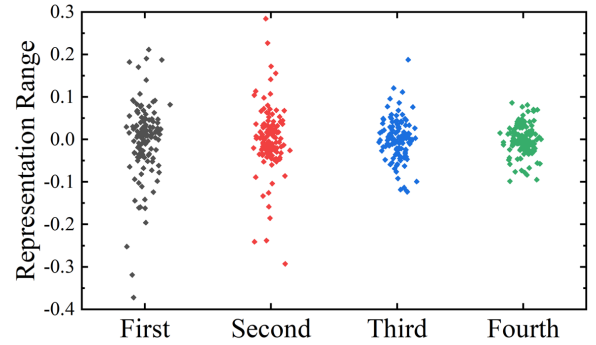


Figure 2: The representation range of the principal components of the standard convolution kernel. The vertical axis stands for the representation range and the horizontal axis represents the first four components of the standard convolution kernels after PCA. Components with a larger range imply stronger representation ability.

correlation of standard kernels along the channel dimension. Considering this, we attempt to generate a kernel space that can approximate the standard convolution kernel by the linear combination of basis vectors, thereby alleviating the problem of computational parameters.

## 3 Methodology

In what follows, we will first give several Definitions and one Lemma, then further propose our SpanKernel base on them.

### 3.1 Background and Definitions

**The Preparation of Linear Algebra.** To illustrate the given method, we need to first present some basic concepts in linear algebra, which can be found from the book in [Meyer, 2000]

**Definition 1.** If  $\beta = \{v_1, v_2, \dots, v_r\}$  is  $r$  linearly independent vectors in  $\mathbb{R}^{k^2}$ , then we have the space spanning:

$$\begin{aligned} \text{Span}\{\beta\} &= \text{Span}\{v_1, v_2, \dots, v_r\} \\ &= \left\{ \sum_{i=1}^r \lambda_i v_i \mid \lambda_i \in \mathbb{R} \right\}. \end{aligned} \quad (1)$$

By Definition 1, we then define the Definition 2,

**Definition 2.** If  $v_i \in \mathbb{R}^{k^2}$ ,  $\lambda_i \in \mathbb{R}$ , and  $r \leq k^2$  where  $r, k^2 \in \mathbb{N}$ , then the following space

$$\mathcal{L}_r = \left\{ \sum_{i=1}^r \lambda_i v_i \mid \lambda_i \in \mathbb{R}, v_i \in \mathbb{R}^{k^2}, r \leq k^2 \right\}, \quad (2)$$

is a subspace of  $\mathbb{R}^{k^2}$ .

**Lemma 1.** In Definition 2, if  $r = k^2$ , the space  $\mathcal{L}_r$  could completely represent  $\mathbb{R}^{k^2}$ , when  $r < k^2$ , the space  $\mathcal{L}_r$  could not completely represent  $\mathbb{R}^{k^2}$ .

By Definition 1, Definition 2 and Lemma 1, we use them into the analysis for the kernel space, and we get the following Definition 3 and three important conclusions.

**Definition 3.** For easy analysis, we may reshape the  $F_i \in \mathbb{R}^{C_{in} \times k \times k}$  to  $C_{in}$  kernel vector  $k_j \in \mathbb{R}^{k^2}$ , correspondingly define the following kernel space:

$$\mathcal{K} = \left\{ k_j \mid j = 1, 2, \dots, C_{in}, k_j \in \mathbb{R}^{k^2}, C_{in} \in \mathbb{N} \right\}, \quad (3)$$

which are distributed in  $\mathbb{R}^{k^2}$ .

According to Definition 2 and Lemma 1, we define  $v_i = \bar{K}_i$ , if  $\beta = \{\bar{K}_1, \bar{K}_2, \dots, \bar{K}_r\}$  is  $r$  linearly independent vectors in  $\mathbb{R}^{k^2}$  kernel space:

**Standard Kernel.** For standard kernel, the parameters in one layer is  $C_{out} \times C_{in} \times k^2$ , where the  $C_{out}$  is represents the number of output channel. Any of kernel vector in standard kernel space can be represented by linearly independent vectors in  $\beta$  when  $r = k^2$ , as the Fig. 1 (b) shows.

**BlueKernel.** In order to reduce parameters, the BlueKernel [Haase and Amthor, 2020] takes an extreme approach. It only learns a  $\bar{K}_1 \in \mathbb{R}^{k^2}$  as basis vector. Then, using the  $C_{in}$  learnt coefficients, the authors expand the basis vector to  $C_{in}$  convolution kernels. In mathematics, its essence is equal to the linear subspace spanned by  $\beta$  when  $r = 1$ , as illustrated in Fig. 1 (d). Considering the parameters for the coefficients, the parameters of BlueKernel in a layer are  $C_{out} \times (C_{in} \times 1 + k^2 \times 1)$ , which are tiny. And as far as we know, the paper of BSConv did not describe its method in terms of math theory.

**SpanKernel.** For the proposed SpanKernel, we have known only two linearly independent vectors ( $\beta$  when  $r = 2$ ) can greatly represent the standard kernel space according to the PCA analysis in Sec. 2, as Figure. 1 (c) shows. Its specific generation method is displayed in Fig. 3. The parameters of SpanKernel in a layer are  $C_{out} \times (C_{in} \times 2 + k^2 \times 2)$ . And it can be concluded from Fig. 1 (c) and (d), the representation ability of SpanKernel is better than BlueKernel prominently.

### 3.2 Generation of SpanKernel

By the above analysis, we intend to only learn two independent kernels as the bases<sup>1</sup>, then extend the two basis kernels  $\bar{K}_i$ ,  $i = 1, 2$  to  $C_{in}$  channels by learnable coefficients and

<sup>1</sup>The case of more independent kernels will be discussed in the experiments.

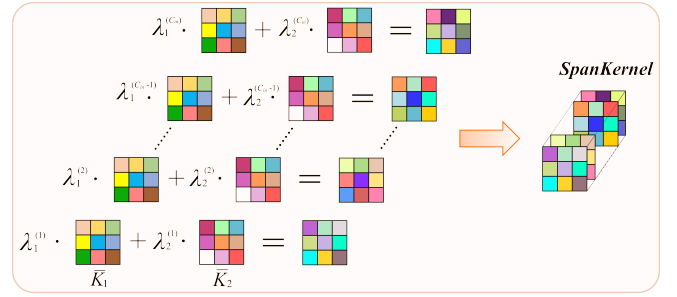


Figure 3: Generation detail of SpanKernel. We first generate two navigated kernels, denoted as  $\bar{K}_1$  and  $\bar{K}_2$ , then extend them to  $C_{in}$  channels with learnable coefficients  $\lambda_1^{(j)}$  and  $\lambda_2^{(j)}$  ( $j = 1, 2, \dots, C_{in}$ ). It is clear that the SpanKernel is formulated by the linear combination of two navigated kernels, which is consistent with the definition in Fig. 1 (c).

finally span the two sets of navigated kernels by their linear combination to construct the so-called SpanKernel, aiming to represent all standard kernels approximately with tolerable errors. For the detailed procedure, please refer to Fig. 3.

### 3.3 Analysis

**The Selection of the Number of Navigated Kernels.** Here, we discuss the number of navigated kernels in different situations. We reshape and view the kernel  $F_i \in \mathbb{R}^{C_{in} \times k \times k}$  to  $F_i \in \mathbb{R}^{C_{in} \times k^2}$  in each input feature channel as a set of vectors, as illustrated in Fig. 1 (a), where  $i$  indicates the output channel index. Usually,  $F_i$  is a non-full-rank matrix, thus satisfying  $\text{Rank}(F_i) \leq k^2$  (generally,  $C_{in} > k^2$ ).

When  $\text{Rank}(F_i) = k^2$ , as mentioned in Sec. 3.1, we could employ  $r = k^2$  independent vectors to completely represent any vector of  $F_i$ . Thus, the number of navigated kernel vectors, i.e.,  $N$ , is also equal to  $\text{Rank}(F_i) = k^2$ . In this situation, the number of parameters with SpanConv is  $C_{out} \times (C_{in} \times k^2 + k^2 \times k^2)$ , which is greater than that with standard convolution,  $C_{out} \times C_{in} \times k^2$ .

When  $\text{Rank}(F_i) < k^2$ , the  $N$  still needs to be equal to  $\text{Rank}(F_i)$  for representing standard kernel space.

In summary, the  $N$  is always equal to  $\text{Rank}(F_i)$ , and the number of parameters will reduce when the  $N$  decreases. To balance the representation ability discussed in the Sec. 2 and the parameters, we finally set  $N = 2$  in our experiments.

**Comparison with Benchmark Convolution Kernels.** With the above background, we analyze the modeling process of SpanKernel and compare it with standard kernel and prior module BlueKernel [Haase and Amthor, 2020] as follows.

For standard convolutions, the kernel in an output channel is arbitrarily scattered in  $\mathbb{R}^{k^2}$  space. In the training process, the algorithm directly learns a set of *fixed* kernel vectors by back-propagation, as Fig. 1 (b) shows. It is self-evident from knowledge of linear algebra that a collection of linearly independent bases is capable of describing any vector in its corresponding space. In the proposed method, we view the kernel vectors that exist in the subspace of the  $\mathbb{R}^{k^2}$  space, and use a pair of navigated vectors to span this subspace, as Fig. 1 (c) illustrates. If the kernel generation has single navigated

| Kernel Type     | Parameters                |
|-----------------|---------------------------|
| Standard Kernel | $C_{out}C_{in}k^2$        |
| SpanKernel      | $C_{out}(2k^2 + 2C_{in})$ |
| BlueKernel      | $C_{out}(k^2 + C_{in})$   |

Table 1: The parameters of the three types of kernels.

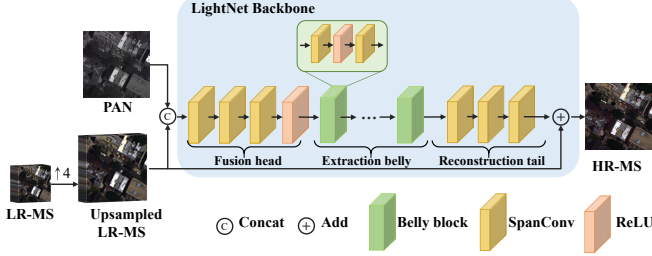


Figure 4: The overall architecture of the LightNet.

kernel, our SpanKernel degenerates into BlueKernel, as Fig. 1 (d) shows. This operation can further reduce the parameters, however, its representation capability is limited. The parameters of the three kernels are displayed in Tab. 1.

### 3.4 Proposed LightNet

In this section, we introduce the proposed LightNet, in which all convolutions are implemented by SpanConv that are realized by replacing the standard kernel with SpanKernel. As shown in Fig. 4, our model has three components, *i.e.*, a fusion head, an extraction belly and a reconstruction tail.

The fusion head consists of three convolution layers with an increasing channel number. It inputs concatenated PAN and upsampled LR-MS images and outputs a preliminary fusion feature. The  $C_{out} \times C_{in}$  of three layers are  $9 \times 9$ ,  $20 \times 9$  and  $32 \times 20$ , respectively. To introduce fractional linearity, a ReLU layer is set at the end of the fusion head.

The extraction belly receives features from the visual backbone and performs detail extraction. It is composed by several belly blocks. Each block is made up of two convolution layers with a sandwiched ReLU layer. The  $C_{out} \times C_{in}$  of the convolution layer in belly are all  $32 \times 32$ , and the block number defaults to 2.

The part of reconstruction tail comprises three convolution layers with decreasing channel number. It produces compensated features, which are added to the upsampled LR-MS image for the final fusion outcome. In particular, the  $C_{out} \times C_{in}$  of the three layers are  $16 \times 32$ ,  $8 \times 16$  and  $8 \times 8$ , respectively.

**Network Training.** Our overall objective is to train LightNet to perform the fusion of LR-MS and PAN images, and obtain a high quality HR-MS image. We exploit the  $\ell_1$  distance between the network prediction and the ground truth (GT) image to supervise the reconstruction process. Besides, the Adam optimizer is utilized with a learning rate that decays by 0.75 every 120 epochs. The initial learning rate and training period are 0.0025 and 800 epochs, respectively. More details are described in the supplementary material.

## 4 Experiments

### 4.1 Compared Methods

We compare our LightNet with recent benchmark DL-based pansharpening methods, *i.e.*, DRPNN [Ghazali *et al.*, 2011], MSDCNN [Wei *et al.*, 2017], BDPN [Zhang *et al.*, 2019], DiCNN [He *et al.*, 2019], PNN [Masi *et al.*, 2016], LPPN [Jin *et al.*, 2022] and FusionNet [Deng *et al.*, 2021]. For each network, we use default hyperparameters mentioned in their original papers. In addition, we also compare with several representative hand-crafted feature-based methods, including BT-H [Lolli *et al.*, 2017], BDSD-PC [Vivone, 2019] and MTF-GLP-FS [Vivone *et al.*, 2018].

### 4.2 Datasets and Evaluation Metrics

**Datasets.** All DL networks are trained and tested on WorldView-3 dataset with eight bands and QuickBird dataset with four bands which are available on the public website<sup>2</sup>. After downloading these datasets, we use Wald’s protocol to simulate 10000 PAN/MS/GT image pairs with sizes of  $64 \times 64$ ,  $16 \times 16 \times 8$ , and  $64 \times 64 \times 8$ , respectively, and divide them into 90%/10% for training (9000 examples) and validation (1000 examples). For testing datasets, the same way as training dataset is taken. Especially, the upsampled MS image (called EXP from hereon) is obtained via a polynomial kernel with 23 coefficients [Aiazzi *et al.*, 2002].

**Evaluation Metrics.** The performance assessment is conducted both at reduced- and full-resolutions. For the quality evaluation of reduced-resolution datasets, we take three commonly used metrics, *i.e.*, the spectral angle mapper (SAM) [Boardman, 1993], the relative dimensionless global error in synthesis (ERGAS) [Wald, 2002] and the Q4 for four-band data or Q8 for eight-band data [Alparone *et al.*, 2004; Garzelli and Nencini, 2009]. For the full-resolution datasets, to assess the performance of all involved methods without GT images, the quality with no reference (QNR) [Alparone *et al.*, 2008], the spatial distortion index  $D_s$  and the spectral distortion index  $D_\lambda$  are employed for the quality evaluation. Especially, the ideal values for QNR, Q4 and Q8 are 1, while for ERGAS, SAM,  $D_s$ , and  $D_\lambda$  are 0.

### 4.3 Assessment on Reduced-Resolution Examples

Quantitative results of compared methods and LightNet on 130 WorldView-3 testing examples are presented in Tab. 2. Besides, we perform the same experiment on 130 QuickBird testing examples with four bands. Also, the number of parameters for these methods is reported on the right side of the table. It can be observed that the parameters of LightNet are significantly smaller compared to other DL-based techniques. Although with the fewest parameters, the performance of the LightNet still surpasses most of the DL-based methods. This well proves the effectiveness of the LightNet, which can maximize the feature representation capacity. For visual comparisons, please refer to supplementary material.

<sup>2</sup><https://www.maxar.com/product-samples/>,  
<https://earth.esa.int/eogateway/catalog/quickbird-full-archive>

| Methods    | WorldView-3        |                    |                    |            | QuickBird          |                    |                    |            |
|------------|--------------------|--------------------|--------------------|------------|--------------------|--------------------|--------------------|------------|
|            | Q8                 | SAM                | ERGAS              | Params     | Q4                 | SAM                | ERGAS              | Params     |
| EXP        | 0.577±0.092        | 8.973±1.605        | 8.102±2.482        | —          | 0.743±0.057        | 4.549±1.141        | 4.011±0.660        | —          |
| BT-H       | 0.873±0.066        | 7.307±1.168        | 4.228±0.881        | —          | 0.867±0.038        | 3.737±1.029        | 2.971±0.526        | —          |
| BDS-PC     | 0.856±0.071        | 8.403±1.397        | 4.578±0.971        | —          | 0.868±0.030        | 4.071±1.060        | 3.192±0.505        | —          |
| MTF-GLP-FS | 0.855±0.069        | 8.401±1.580        | 4.659±1.029        | —          | 0.850±0.036        | 4.064±1.178        | 3.296±0.577        | —          |
| DRPNN      | 0.906±0.062        | 5.094±0.783        | 3.046±0.545        | 1867K      | 0.949±0.019        | 2.075±0.444        | 1.814±0.309        | 418K       |
| MSDCNN     | 0.900±0.067        | 5.564±0.792        | 3.235±0.544        | 229K       | 0.949±0.019        | 2.065±0.452        | 1.831±0.306        | 190K       |
| BDPN       | 0.898±0.064        | 5.932±0.925        | 3.410±0.629        | 1487K      | 0.922±0.024        | 2.553±0.572        | 2.301±0.402        | 1481K      |
| DiCNN      | 0.912±0.057        | 5.075±0.760        | 3.006±0.586        | 47K        | 0.949±0.019        | 2.059±0.455        | 1.852±0.327        | 43K        |
| PNN        | 0.890±0.078        | 5.902±0.916        | 3.353±0.533        | 104K       | 0.946±0.019        | 2.144±0.473        | 1.882±0.313        | 80K        |
| LPPN       | 0.903±0.067        | 5.159±0.775        | 3.065±0.531        | 51K        | 0.957±0.018        | 1.933±0.378        | 1.664±0.260        | 160K       |
| FusionNet  | <b>0.920±0.053</b> | <b>4.561±0.731</b> | <b>2.724±0.533</b> | 79K        | <b>0.958±0.017</b> | <b>1.821±0.374</b> | <b>1.629±0.283</b> | 76K        |
| LightNet   | 0.919±0.053        | 4.897±0.792        | 2.901±0.554        | <b>16K</b> | <b>0.958±0.016</b> | 1.842±0.389        | 1.663±0.273        | <b>16K</b> |

Table 2: Average quantitative comparisons on 130 reduced-resolution WorldView-3 and QuickBird examples. Best results are in boldface.

| Methods    | WorldView-3        |                    |                    |            | QuickBird          |                    |                    |            |
|------------|--------------------|--------------------|--------------------|------------|--------------------|--------------------|--------------------|------------|
|            | $D_\lambda$        | $D_s$              | QNR                | Params     | $D_\lambda$        | $D_s$              | QNR                | Params     |
| EXP        | 0.055±0.014        | 0.141±0.031        | 0.813±0.036        | —          | 0.047±0.005        | 0.150±0.038        | 0.811±0.038        | —          |
| BT-H       | 0.093±0.029        | 0.096±0.043        | 0.821±0.057        | —          | 0.088±0.030        | 0.100±0.033        | 0.822±0.050        | —          |
| BDS-PC     | 0.158±0.028        | <b>0.036±0.040</b> | 0.813±0.050        | —          | 0.121±0.028        | 0.041±0.028        | 0.843±0.043        | —          |
| MTF-GLP-FS | <b>0.040±0.017</b> | 0.081±0.040        | 0.884±0.050        | —          | <b>0.036±0.011</b> | 0.108±0.031        | 0.860±0.038        | —          |
| DRPNN      | 0.119±0.028        | 0.050±0.030        | 0.838±0.046        | 1867K      | 0.068±0.027        | 0.033±0.017        | 0.901±0.036        | 418K       |
| MSDCNN     | 0.160±0.049        | 0.069±0.031        | 0.783±0.064        | 229K       | 0.080±0.045        | 0.030±0.013        | 0.893±0.053        | 190K       |
| BDPN       | 0.133±0.039        | 0.067±0.026        | 0.810±0.054        | 1487K      | 0.064±0.026        | 0.077±0.027        | 0.864±0.043        | 1481K      |
| DiCNN      | 0.105±0.036        | 0.094±0.025        | 0.811±0.039        | 47K        | 0.095±0.041        | 0.116±0.042        | 0.801±0.066        | 43K        |
| PNN        | 0.143±0.071        | 0.083±0.012        | 0.787±0.070        | 104K       | 0.107±0.053        | 0.065±0.030        | 0.836±0.071        | 80K        |
| LPPN       | 0.122±0.034        | 0.058±0.012        | 0.827±0.039        | 51K        | 0.067±0.020        | 0.022±0.010        | 0.912±0.025        | 160K       |
| FusionNet  | 0.093±0.047        | 0.083±0.026        | 0.833±0.053        | 79K        | 0.041±0.013        | <b>0.020±0.009</b> | <b>0.940±0.017</b> | 76K        |
| LightNet   | 0.054±0.017        | 0.042±0.031        | <b>0.907±0.042</b> | <b>16K</b> | 0.051±0.026        | 0.032±0.015        | 0.919±0.037        | <b>16K</b> |

Table 3: Average quantitative comparisons on 64 full-resolution WorldView-3 and QuickBird examples. Best results are in boldface.

| Network     | Q8                 | SAM                | ERGAS              | Params     |
|-------------|--------------------|--------------------|--------------------|------------|
| DiCNN       | <b>0.912±0.057</b> | <b>5.075±0.760</b> | <b>3.006±0.586</b> | 83K        |
| DiCNN+      | 0.886±0.072        | 6.853±1.096        | 3.767±0.703        | <b>16K</b> |
| DiCNN++     | 0.891±0.072        | 6.445±1.026        | 3.575±0.607        | 28K        |
| FusionNet   | <b>0.920±0.053</b> | <b>4.561±0.731</b> | <b>2.724±0.533</b> | 79K        |
| FusionNet+  | 0.891±0.074        | 6.226±0.987        | 3.478±0.578        | <b>12K</b> |
| FusionNet++ | 0.904±0.065        | 5.384±0.828        | 3.131±0.551        | 24K        |

Table 4: The performance of SpanConv and BSConv as the embedded modules in benchmark networks.

#### 4.4 Assessment on Full-Resolution Examples

We also perform test on full-resolution datasets where most DL-based methods fail to generate reasonable results due to the over-fitting. The results are shown in Tab. 3. As expected, some hand-crafted feature-based methods surpass the DL-based methods in several metrics, and BDS-PC and MTF-GLP-FS win the best performance in  $D_\lambda$  and  $D_s$  on WorldView-3 datasets, respectively. Nevertheless, our gains are higher than other DL-based methods, closing to the level of the best in all metrics, which verifies the SpanConv can overcome the defect that deep learning has a large gap between the performance of real data and simulation data.

#### 4.5 Discussion

**Network Generalization.** It is well known that DL-based approaches have poor generality. For further verification with the generalization of the LightNet, we test the models trained in WorldView-3 datasets on 12 WorldView-2 examples in different places. The results are displayed in Tab. 5. It can be observed that the proposed LightNet outperforms all DL-based algorithms with the fewest parameters in generalization. Because more complicated models are more prone to dataset changes. Thus, the tiny model size of LightNet contributes to its high generalization ability.

**As Embedded Module.** As an embedded module, SpanConv can be embedded into other benchmark networks to replace standard convolution. We test the SpanConv as embedded module in the DiCNN and FusionNet, and compare it with BSConv. The results are shown in Tab. 4. The symbol "+" means the network embedded with BSConv, and "++" means the network embedded with SpanConv. It can be observed that the network using SpanConv and BSConv all reduces the parameters. SpanConv, unlike BSConv, may enhance performance by increasing parameters. This indicates that SpanConv's kernel space may be approximated to conventional convolution for nonlinear characterization.

| Method    | Q8                 | SAM                | ERGAS              | Params     |
|-----------|--------------------|--------------------|--------------------|------------|
| EXP       | 0.581±0.057        | 7.494±1.239        | 7.029±0.827        | -          |
| DRPNN     | 0.692±0.074        | 9.284±0.552        | 8.042±0.336        | 1867K      |
| MSDCNN    | 0.630±0.118        | 9.545±0.686        | 7.983±0.259        | 229K       |
| BDPN      | 0.700±0.130        | 10.150±0.485       | 8.123±0.386        | 1487K      |
| DiCNN     | 0.561±0.080        | 9.166±0.940        | 8.075±0.312        | 47K        |
| PNN       | 0.619±0.173        | 13.173±0.750       | 8.086±0.327        | 104K       |
| LPPN      | 0.663±0.117        | 8.690±0.658        | 7.139±0.273        | 51K        |
| FusionNet | 0.663±0.092        | 8.111±0.927        | 6.265±0.412        | 79K        |
| LightNet  | <b>0.828±0.057</b> | <b>6.160±0.999</b> | <b>4.155±0.495</b> | <b>16K</b> |

Table 5: Average quantitative comparisons on 12 WorldView-2 examples in different places. Best results are in boldface.

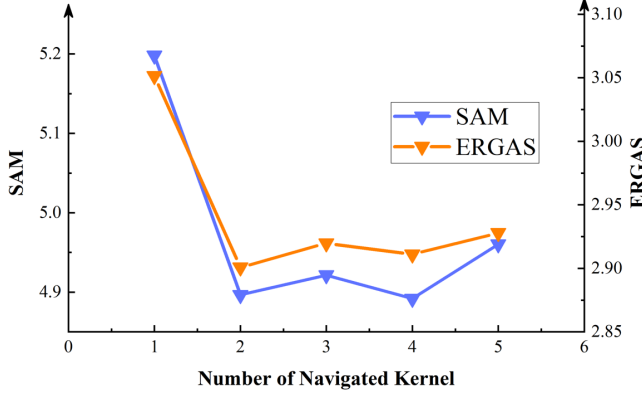


Figure 5: The SAM and ERGAS curves with varying navigated kernel number  $N$  for LightNet.

**The Number of the Navigated Kernels.** In the previous discussion, we set navigated kernel number as 2. In this section, we will justify this setting to see what happens. We have tested the performance of LightNet with different numbers of the navigated kernels. The results are reported in Fig. 5. It is worth to mention that when  $N$  is set to 1, the SpanConv degenerates into BSConv. The most obvious improvement is achieved when  $N$  increasing from 1 to 2, and metrics become fluctuate when  $N > 2$ , which indicates two navigated kernels are enough to construct a qualified kernel space for pansharpening. In addition, during the experiment, we find that the optimized  $N$  differs in the different networks and tasks.

**The Computational Cost of the Networks.** The computational cost of benchmark DL-based methods is presented in Tab. 6. It can be observed that LightNet can achieve the satisfying performance with the fewest computational resource.

**The Representation Ability of SpanKernel.** In this section, we hook out the weights of LightNet with SpanConv, BSConv, and standard convolution, respectively. And we use  $\ell_2$  distance and Pearson coefficient to measure the difference between the SpanKernel, BlueKernel and the standard convolution kernel. From the results displayed in Tab. 7, the difference of the kernels gradually decrease as the network flows to the end, indicating the correlation become prominent as the networks deepens. In the shallow layer of the network, the difference of SpanKernel and standard convolution kernel are much smaller than that of BlueKernel, illustrating that the

| Network   | Params     | FLOPS        | MAdd          |
|-----------|------------|--------------|---------------|
| DRPNN     | 1867K      | 1.8G         | 3.6G          |
| MSDCNN    | 229K       | 936.2M       | 1.9G          |
| BDPN      | 1487K      | 3.8G         | 7.6G          |
| DiCNN     | 47K        | 191.9M       | 382.5M        |
| PNN       | 104K       | 299.9M       | 599.1M        |
| FusionNet | 79K        | 322.7M       | 642.4M        |
| LightNet  | <b>16K</b> | <b>67.0M</b> | <b>126.4M</b> |

Table 6: The computational cost comparison of all networks.

| Metrics     | $\ell_2$ distance |              | Pearson      |              |
|-------------|-------------------|--------------|--------------|--------------|
| Layer Name  | BlueKernel        | SpanKernel   | BlueKernel   | SpanKernel   |
| head_conv1  | 3.040             | <b>2.870</b> | 0.032        | <b>0.068</b> |
| head_conv2  | 0.354             | <b>0.256</b> | 0.004        | <b>0.011</b> |
| head_conv3  | <b>0.335</b>      | 0.426        | 0.016        | <b>0.021</b> |
| belly_conv1 | 0.625             | <b>0.602</b> | 0.010        | <b>0.011</b> |
| belly_conv2 | 0.084             | <b>0.073</b> | <b>0.016</b> | 0.003        |
| belly_conv3 | <b>0.060</b>      | 0.158        | 0.011        | <b>0.012</b> |
| belly_conv4 | <b>0.030</b>      | 0.031        | <b>0.012</b> | 0.004        |
| tail_conv1  | <b>0.008</b>      | 0.009        | 0.007        | <b>0.010</b> |
| tail_conv2  | <b>0.002</b>      | <b>0.002</b> | <b>0.057</b> | 0.039        |
| tail_conv3  | 0.002             | <b>0.001</b> | <b>0.111</b> | 0.049        |

Table 7: The comparison of the error of SpanKernel and BlueKernel.

kernel space constructed by Spanconv is closer to the standard kernel space. In the other word, compared with BlueKernel, Spanconv can describe richer mapping relationships, thus it has stronger feature representation capabilities.

**Limitations.** When the kernels have strong independence, the representation ability of our SpanKernel will be limited. As a result, when the kernels display a high degree of dependence fit with the SpanKernel assumption, our technique performs well, consistent with the experimental results.

## 5 Conclusion

Standard convolution has a high computational cost primarily because the dimension of the convolution kernel is proportional to the channel count of the feature maps. The proposed method introduces a novel convolution operation, SpanConv, that constructs the kernel space by spanning a small number of navigated kernels. A simple end-to-end learning framework, *i.e.*, LightNet, is presented for remote sensing pansharpening task based on the SpanConv. The comparison to the state-of-the-art method demonstrates that our method, to the best of our knowledge, requires the fewest network parameters for pansharpening and achieves superior generalization when achieving competitive outcomes.

## Acknowledgments

This research is supported by NSFC (12171072, 61876203, 61702083), Key Projects of Applied Basic Research in Sichuan Province (Grant No. 2020YJ0216), and National Key Research and Development Program of China (Grant No. 2020YFA0714001).

## References

- [Aiazzi *et al.*, 2002] Bruno Aiazzi, Luciano Alparone, Stefano Baronti, and Andrea Garzelli. Context-driven fusion of high spatial and spectral resolution images based on oversampled multiresolution analysis. *IEEE Transactions on Geoscience and Remote Sensing*, 40(10):2300–2312, 2002.
- [Alparone *et al.*, 2004] Luciano Alparone, Stefano Baronti, Andrea Garzelli, and Filippo Nencini. A global quality measurement of pan-sharpened multispectral imagery. *IEEE Geoscience and Remote Sensing Letters*, 1(4):313–317, 2004.
- [Alparone *et al.*, 2008] Luciano Alparone, Bruno Aiazzi, Stefano Baronti, Andrea Garzelli, Filippo Nencini, and Massimo Selva. Multispectral and panchromatic data fusion assessment without reference. *Photogrammetric Engineering & Remote Sensing*, 74(2):193–200, 2008.
- [Boardman, 1993] Joseph Boardman. Automating spectral unmixing of aviris data using convex geometry concepts. In *Summaries of the 4th Annual JPL Airborne Geoscience Workshop*, volume 1, pages 11–14, 1993.
- [Deng *et al.*, 2021] Liang-Jian Deng, Gemine Vivone, Cheng Jin, and Jocelyn Chanussot. Detail injection-based deep convolutional neural networks for pansharpening. *IEEE Transactions on Geoscience and Remote Sensing*, 59(8):6995–7010, 2021.
- [Garzelli and Nencini, 2009] Andrea Garzelli and Filippo Nencini. Hypercomplex quality assessment of multi/hyperspectral images. *IEEE Geoscience and Remote Sensing Letters*, 6(4):662–665, 2009.
- [Ghazali *et al.*, 2011] Rozaida Ghazali, Abir Jaafar Hussain, and Panos Liatsis. Dynamic ridge polynomial neural network: Forecasting the univariate non-stationary and stationary trading signals. *Expert Systems with Applications*, 38(4):3765–3776, 2011.
- [Haase and Amthor, 2020] Daniel Haase and Manuel Amthor. Rethinking depthwise separable convolutions: How intra-kernel correlations lead to improved MobileNets. In *The IEEE/CVF Conference on Computer Vision and Pattern Recognition (CVPR)*, June 2020.
- [He *et al.*, 2019] Lin He, Yizhou Rao, Jun Li, Jocelyn Chanussot, Antonio Plaza, Jiawei Zhu, and Bo Li. Pansharpening via detail injection based convolutional neural networks. *IEEE Journal of Selected Topics in Applied Earth Observations and Remote Sensing*, 12(4):1188–1204, 2019.
- [Howard *et al.*, 2017] Andrew G. Howard, Menglong Zhu, Bo Chen, Dmitry Kalenichenko, Weijun Wang, Tobias Weyand, Marco Andreetto, and Hartwig Adam. Mobilenets: Efficient convolutional neural networks for mobile vision applications. *arXiv preprint arXiv:1704.04861*, 2017.
- [Jin *et al.*, 2022] Cheng Jin, Liang-Jian Deng, Ting-Zhu Huang, and Gemine Vivone. Laplacian pyramid networks: A new approach for multispectral pansharpening. *Information Fusion*, 78:158–170, 2022.
- [Krizhevsky *et al.*, 2012] Alex Krizhevsky, Ilya Sutskever, and Geoffrey E Hinton. Imagenet classification with deep convolutional neural networks. *Advances in neural information processing systems*, 25:1097–1105, 2012.
- [Lolli *et al.*, 2017] Simone Lolli, Luciano Alparone, Andrea Garzelli, and Gemine Vivone. Haze correction for contrast-based multispectral pansharpening. *IEEE Geoscience and Remote Sensing Letters*, 14(12):2255–2259, 2017.
- [Masi *et al.*, 2016] Giuseppe Masi, Davide Cozzolino, Luisa Verdoliva, and Giuseppe Scarpa. Pansharpening by convolutional neural networks. *Remote Sensing*, 8(7):594, 2016.
- [Meyer, 2000] C. D. Meyer. *Matrix Analysis and Applied Linear Algebra Book and Solutions Manual*. Matrix Analysis and Applied Linear Algebra Book and Solutions Manual, 2000.
- [T.-J. Zhang and Vivone, 2022] T.-Z. Huang J. Chanussot T.-J. Zhang, L.-J. Deng and G. Vivone. A triple-double convolutional neural network for panchromatic sharpening. *IEEE Transactions on Neural Networks and Learning Systems*, 2022.
- [Vivone *et al.*, 2018] Gemine Vivone, Rocco Restaino, and Jocelyn Chanussot. Full scale regression-based injection coefficients for panchromatic sharpening. *IEEE Transactions on Image Processing*, 27(7):3418–3431, 2018.
- [Vivone *et al.*, 2020] Gemine Vivone, Mauro Dalla Mura, Andrea Garzelli, Rocco Restaino, Giuseppe Scarpa, Magnus Orn Ulfarsson, Luciano Alparone, and Jocelyn Chanussot. A new benchmark based on recent advances in multispectral pansharpening: Revisiting pansharpening with classical and emerging pansharpening methods. *IEEE Geoscience and Remote Sensing Magazine*, 2020.
- [Vivone, 2019] Gemine Vivone. Robust band-dependent spatial-detail approaches for panchromatic sharpening. *IEEE transactions on Geoscience and Remote Sensing*, 57(9):6421–6433, 2019.
- [Wald, 2002] Lucien Wald. *Data fusion: definitions and architectures: fusion of images of different spatial resolutions*. Presses des MINES, 2002.
- [Wei *et al.*, 2017] Yancong Wei, Qiangqiang Yuan, Xiangchao Meng, Huanfeng Shen, Liangpei Zhang, and Michael Ng. Multi-scale-and-depth convolutional neural network for remote sensed imagery pan-sharpening. In *2017 IEEE International Geoscience and Remote Sensing Symposium (IGARSS)*, pages 3413–3416. IEEE, 2017.
- [Yang *et al.*, 2017] Junfeng Yang, Xueyang Fu, Yuwen Hu, Yue Huang, Xinghao Ding, and John Paisley. Pannet: A deep network architecture for pan-sharpening. In *Proceedings of the IEEE/CVF International Conference on Computer Vision*, pages 5449–5457, 2017.
- [Zhang *et al.*, 2019] Yongjun Zhang, Chi Liu, Mingwei Sun, and Yangjun Ou. Pan-sharpening using an efficient bidirectional pyramid network. *IEEE Transactions on Geoscience and Remote Sensing*, 57(8):5549–5563, 2019.